Insights into the molecular basis for substrate binding and specificity of the wild-type L-arginine/agmatine antiporter AdiC

Hüseyin Ilgü[a,b,1], Jean-Marc Jeckelmann[a,b,1], Vytautas Gapsys[c], Zöhre Ucurum[a,b], Bert L. de Groot[c], and Dimitrios Fotiadis[a,b,2]

[a]Institute of Biochemistry and Molecular Medicine, University of Bern, CH-3012 Bern, Switzerland; [b]Swiss National Centre of Competence in Research TransCure, University of Bern, CH-3012 Bern, Switzerland; and [c]Computational Biomolecular Dynamics Group, Max-Planck-Institute for Biophysical Chemistry, D-37077 Goettingen, Germany

Pathogenic enterobacteria need to survive the extreme acidity of the stomach to successfully colonize the human gut. Enteric bacteria circumvent the gastric acid barrier by activating extreme acid-resistance responses, such as the arginine-dependent acid resistance system. In this response, L-arginine is decarboxylated to agmatine, thereby consuming one proton from the cytoplasm. In *Escherichia coli*, the L-arginine/agmatine antiporter AdiC facilitates the export of agmatine in exchange of L-arginine, thus providing substrates for further removal of protons from the cytoplasm and balancing the intracellular pH. We have solved the crystal structures of wild-type AdiC in the presence and absence of the substrate agmatine at 2.6-Å and 2.2-Å resolution, respectively. The high-resolution structures made possible the identification of crucial water molecules in the substrate-binding sites, unveiling their functional roles for agmatine release and structure stabilization, which was further corroborated by molecular dynamics simulations. Structural analysis combined with site-directed mutagenesis and the scintillation proximity radioligand binding assay improved our understanding of substrate binding and specificity of the wild-type L-arginine/agmatine antiporter AdiC. Finally, we present a potential mechanism for conformational changes of the AdiC transport cycle involved in the release of agmatine into the periplasmic space of *E. coli*.

membrane protein | scintillation proximity assay | substrate binding | transporter | X-ray structure

Enterobacteria from the genera *Escherichia*, *Klebsiella*, *Salmonella*, *Shigella*, and *Yersinia* include members that are human intestinal pathogens. To reach the gut, enteric bacteria have to survive the strongly acidic gastric environment (e.g., pH 1.5–4). Enteric bacteria do so by activating extreme acid-resistance responses (1). The arginine-dependent acid-resistance system of *Escherichia coli* has been extensively studied and is able to keep the cytoplasm above pH 5 during exposure of *E. coli* to an extremely acidic environment. The main actors in this system are the cytoplasmic acid-activated arginine decarboxylase AdiA and the inner membrane L-arginine (Arg)/agmatine (Agm) antiporter AdiC (1), a member of the amino acid/polyamine/organocation (APC) transporter superfamily (2). AdiA decarboxylates Arg to Agm by consuming a proton from the cytoplasm (Fig. 1*A*). The produced Agm carries this "virtual proton" in the form of a C-H bond, which then leaves the bacterium through the antiporter AdiC by exchanging in a 1:1 stoichiometry Agm by Arg from the outside (e.g., from the gastric juice). The free energy of Arg decarboxylation drives the continuous pumping of protons out of the cell (3). Studies on the molecular genetics (4, 5), protein biochemistry (2, 3), transport function (2, 3, 6, 7), and structure (2, 8–11) of AdiC have enriched our understanding of this protein. The four reported 3D AdiC structures consist of 12 transmembrane α-helices (TMs) and are in the outward-open, substrate-free (8, 9), outward-open, Arg-bound (11), and outward-facing occluded

Arg-bound states (10). The two outward-open, substrate-free structures are at the reasonable and moderate resolutions of 3.2 Å (8) and 3.6 Å (9), respectively, and the only ones available of wild-type AdiC (AdiC-wt). The two other structures are with bound Arg and at 3-Å resolution, and could only be obtained as a result of the introduction of specific point mutations: AdiC-N22A (10) and AdiC-N101A (11). The N101A mutation results in a defective AdiC protein unable to bind Arg and with a dramatically decreased turnover rate compared with wild-type (11). It remains unclear how these two functional features comply with the obtained crystal structure of AdiC-N101A in complex with Arg. The specific mutation N22A in AdiC is interesting because this amino acid residue is located near the substrate-binding pocket and increases the affinity of AdiC for Arg approximately sixfold (10). In addition to their great value for the understanding of the molecular working mechanism of AdiC and other APC superfamily transporters, high-resolution structures of AdiC are very useful for homology modeling of human SLC7 family members (12); for example, of the large-neutral amino acid transporter-1 (LAT1; SLC7A5) (13) and -2 (LAT2; SLC7A8) (14, 15). Because structure determination of human transporters—and eukaryotic membrane proteins in general—still represents a major challenge,

Significance

Disease-causing bacteria are able to survive the strongly acidic environment of the stomach by activating extreme acid-resistance responses. One of these responses in gut bacteria consists of converting L-arginine into agmatine, which results in removal of one proton from the cytoplasm. In *Escherichia coli*, the transport protein AdiC assures the efflux of agmatine in exchange with L-arginine. We have solved the structures of wild-type AdiC in the presence and absence of the substrate agmatine at high resolution, allowing for the identification of crucial water molecules and of their functional roles in the substrate-binding pocket. Furthermore, structure-based site-directed mutagenesis combined with a radioligand binding assay improved our understanding of substrate binding and specificity of the L-arginine/agmatine antiporter AdiC.
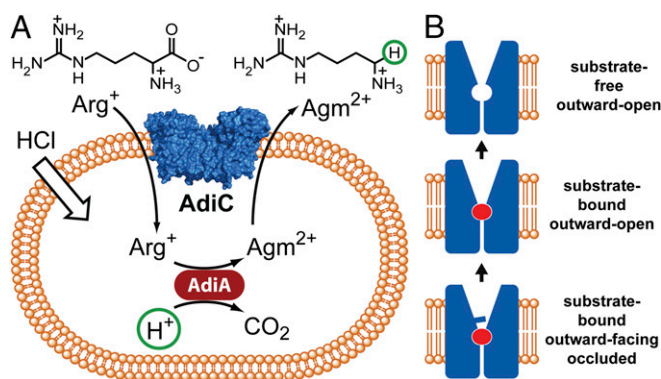
Fig. 1. Physiology and selected conformational states of AdiC. (*A*) Schematic illustration of the arginine-dependent acid-resistance system of *E. coli*. Arg is decarboxylated in the cytoplasm by the acid-activated arginine-decarboxylase AdiA, thereby consuming one proton (circled in green). This virtual proton ends up as C-H bond at the 1-position of the product 1-amino-4-guanidino-*n*-butane (Agm; proton indicated by a green circle). Agm is then removed from the cell through the AdiC-mediated Arg/Agm exchange across the inner membrane. (*B*) Conformational states of AdiC involved in Agm release into the periplasmic space. Arrows indicate the flow of the sequential conformational states. The AdiC monomer is colored in blue and the Agm molecule in red.

homology models based on bacterial homologs are of great interest for understanding transport function and their roles in human health and disease. Recently, a homology model of human LAT1 based on one of the available AdiC crystal structures at 3-Å resolution (10) was built, and used for virtual ligand screening and the successful identification of new inhibitors (13). Such inhibitors are of great interest because LAT1 represents a cancer drug target (12). Importantly, high-resolution structures of AdiC would help in improving the present human LAT1 homology model (13), thus promoting its application for virtual ligand screening.

Here we present the crystal structure of AdiC-wt with bound Agm substrate at 2.6-Å resolution. In addition, the structure of substrate-free AdiC-wt was solved at the unprecedented resolution of 2.2 Å. Both structures were captured in an outward-open state. Importantly, water molecules in the substrate-binding pocket of the two AdiC structures were determined at high resolutions, allowing the exploration of their functional roles. Structure-based site-directed mutagenesis combined with the scintillation proximity radioligand binding assay (16) improved our understanding of the molecular basis for substrate binding and specificity of the AdiC transporter. Finally, based on our results and the previously published outward-facing occluded Arg-bound structure (10), we present a potential mechanism for conformational changes of the AdiC transport cycle (Fig. 1*B*) involved in the release of Agm into the periplasmic space of *E. coli*.

Results

The Agm-Bound and Substrate-Free AdiC-wt Structures. To deepen our understanding on the substrate binding and transport mechanism of AdiC, we determined its structure in complex with Agm at 2.6-Å resolution (see Table S1 for data collection and refinement statistics). In contrast, innumerable attempts to cocrystallize AdiC-wt with Arg failed. This observation might be attributed to the approximately threefold higher affinity of AdiC-wt for Agm compared with Arg as determined by scintillation proximity assay (SPA) (Table 1; see Fig. S1 for raw data). Furthermore, we solved the structure of substrate-free AdiC-wt (^apoAdiC-wt) at the unprecedented resolution of 2.2 Å (see Table S1 for data collection and refinement statistics). Importantly, these two structures at high-resolution made possible the identification of crucial water molecules in the substrate-binding pocket of AdiC in the presence and absence of Agm (see Fig. S2 for electron density maps of this region). Both structures were captured in the outward-open conformation and display subtle structural differences (rmsd 0.28 Å for 437 residues) (Fig. 2). The Agm molecule is bound at the center of the AdiC transport path (Fig. 2), being recognized by several amino acids from TM1, TM3, TM6, TM8, and TM10, mainly by hydrogen bonds (H-bonds) and one cation–π interaction (Fig. 3*A*). Agm consists of chemically different portions: two hydrophilic [i.e., the primary amino group and the guanidinium (Gdm) group] and one hydrophobic (i.e., the aliphatic region connecting the previous two). In the AdiC-wt structure with bound Agm (^AgmAdiC-wt) (see Fig. 2*D* for the omit electron density map of Agm), the primary amino group donates three H-bonds to the backbone carbonyl oxygen atoms of I23 (TM1), S203 (TM6), and I205 (TM6) (Fig. 3*A*). The three nitrogen atoms of the Gdm group of Agm (hereafter referred to as Nε, Nη1, and Nη2) (Fig. 3*A*) interact as follows: Nη1 with the carbonyl oxygen atom of C97 (TM3) and the amide group oxygen atom of N101 (TM3), Nη2 with the carbonyl oxygen atom of A96 (TM3), and Nε with the sulfur atom of M104 (TM3). Importantly, a water molecule (H₂O1) (Fig. 3*A*) was found interacting via H-bonds with Nη2, the carbonyl oxygen atom of A96 (TM3) and the hydroxyl group of S357 (TM10). Thus, H₂O1 is involved in substrate binding and in shaping the binding pocket by stabilizing interactions between TM3 and TM10. The Gdm group of Agm also interacts via a cation–π interaction with W293 (TM8). This interaction was shown to be crucial for substrate binding to AdiC, because the AdiC–W293L mutant is unable to bind and transport substrates (2, 8). Van der Waals interactions with the aliphatic portion of Agm are present with the side chains of I205 (TM6) and W293 (TM8) (Fig. S3*A*).

Degree of Interaction Between Arg and Agm, and Amino Acid residue Side Chains in the Binding Pocket of AdiC-wt. In the ^AgmAdiC-wt structure, interactions between Agm and the side chains of the amino acid residues N101 (TM3), M104 (TM3), I205 (TM6), W293 (TM8), and S357 (TM10) were found (see previous section). To evaluate the importance and involvement of these residues for Arg and Agm binding in AdiC, we replaced the corresponding residues by alanine producing single mutants for binding studies using the SPA. As documented in the literature, replacement of N101 or

Table 1. Ligand binding affinities of AdiC variants

Variant	AdiC-wt K_i (µM)	AdiC-N22A K_i (µM)	AdiC-S26A K_i (µM)	AdiC-M104A K_i (µM)	AdiC-I205A K_i (µM)	AdiC-S357A K_i (µM)
Arg	148 (103–212)	23 (20–27)	154 (86–274)	193 (141–264)	140 (102–192)	176 (121–257)
Agm	56 (38–82)	216 (191–245)	90 (44–183)	107 (78–145)	53 (37–75)	81 (61–107)
Arg-OMe	293 (210–409)	77 (66–89)	1,693 (920–2,534)	N/A	N/A	N/A
Arg-NH₂	864 (467–1,118)	1,816 (1,282–2,572)	1,527 (1,205–2,379)	N/A	N/A	N/A

K_i: inhibition constant (binding affinity). The determined K_i values are from at least three independent experiments, each in triplicate. 95% confidence interval values are indicated in brackets. N/A: not available. Arg (L-arginine), Agm (agmatine), Arg-OMe (L-arginine methyl ester), and Arg-NH₂ (L-arginine amide).
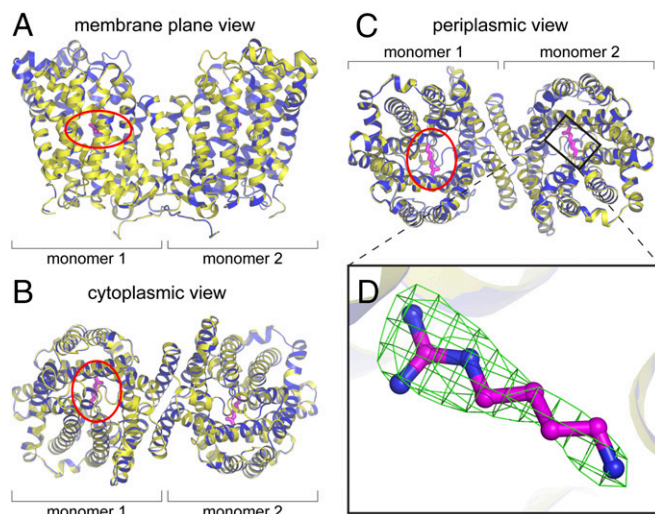
Fig. 2. Cartoon ribbon representations of the Agm-bound and substrate-free AdiC structures. (A–C) Superpositions of ^{Agm}AdiC-wt (in blue) and ^{apo}AdiC-wt (in yellow) dimers. Individual monomers are indicated and transmembrane helices are discerned. The Agm molecule (magenta sticks) bound to ^{Agm}AdiC-wt is shown and is located about at the center of the transport path. The location of the substrate-binding pocket is indicated by red ellipses. Three different views are displayed: view from the membrane plane (A), and from the cytoplasmic (B), and periplasmic sides (C). (D) Omit electron density map at 3.0 σ (green) of the Agm molecule (magenta sticks) bound to ^{Agm}AdiC-wt.

W293 dramatically decreases and mostly even completely abolishes the transport function of AdiC (2, 8, 11). In line with these findings, binding of [³H]Arg to AdiC-N101A and AdiC-W293A was strongly impaired (Fig. S4A). For the AdiC mutants M104A, I205A, and S357A, inhibition constants (K_is) were determined by SPA using [³H]Arg as radioligand, and Arg and Agm as inhibitors (Table 1; see Fig. S4B for raw data). The affinity for Arg was moderately decreased in AdiC-M104A and AdiC-S357A, and was similar in AdiC-I205A when comparing to AdiC-wt (Table 1). For Agm, AdiC-I205A and AdiC-S357A had similar and slightly lower affinities compared with AdiC-wt (Table 1). Interestingly, the affinity of AdiC-M104A for Agm was reduced by about 50% compared with AdiC-wt (Table 1), indicating a significant interaction between the Gdm Nε and the sulfur atom of M104 (TM3) (Fig. 3A). Furthermore, comparison of the K_is of AdiC-M104A and AdiC-wt for Arg and Agm (Table 1) indicates a relatively weaker interaction between the sulfur atom of M104 and Arg compared with Agm.

Comparison of the Substrate-Binding Sites in the Agm-Bound and Substrate-Free AdiC Structures. Fig. 3 compares the substrate-binding sites of the ^{Agm}AdiC-wt and ^{apo}AdiC-wt structures. Whereas the crystallographic water molecule H_2O1 is present in both structures, three additional ones (i.e., H_2O2, H_2O3, and H_2O4) were found in the ^{apo}AdiC-wt structure (Fig. 3B). Importantly, these additional water molecules mimic most of the hydrophilic portions of Agm. Specifically, H_2O2 in the ^{apo}AdiC-wt structure is located near the position of Nη1 in the ^{Agm}AdiC-wt structure, thus replacing the H-bonds of Nη1 with the protein (Fig. 3). In contrast, the previously observed H-bonds of Nη2 with the protein and H_2O1 are not replaced by H_2O3 in the ^{apo}AdiC-wt structure, H_2O3 only being within H-bond distance with H_2O2 (see distances in Fig. 3B). Similarly, H_2O4 also replaces a nitrogen atom of the Agm molecule (i.e., the nitrogen atom of the primary amino group) and its H-bonds to the protein (Fig. 3).

As mentioned above, subtle differences were found between the ^{Agm}AdiC-wt and ^{apo}AdiC-wt structures (Fig. 2). Nevertheless, a significant difference in the substrate-binding pocket is the rotamer conformation of M104 (TM3). Whereas in the ^{apo}AdiC-wt structure,

the methylmercapto group of M104 (TM3) is protruding into the substrate-binding pocket, this methionine residue adopts a different conformation in the ^{Agm}AdiC-wt structure exposing its sulfur atom as hydrogen acceptor for Nε (Fig. 3; see Fig. S2 for electron density of M104 rotamers). NH⋯S H-bonds are present in numerous structures contributing to protein stability (17, 18).

Presence of Water Molecules in the Substrate-Binding Pocket of ^{apo}AdiC-wt at Human Body Temperature. To evaluate if the water molecules (i.e., H_2O1–H_2O4) identified in the ^{apo}AdiC-wt structure at cryogenic temperature also exist at normal human internal body temperature, (i.e., 37 °C), we performed molecular dynamics (MD) simulations at this temperature. Fig. S5A depicts the water density maps calculated by MD simulations. Water densities for the molecules H_2O2–H_2O4 in the ^{apo}AdiC-wt MD simulations coincide well with the crystallographic water positions (Fig. S5A). The crystallographically resolved water molecule H_2O1 is partially covered by the solvent densities from MD simulations. The density corresponding to H_2O1 is present, but appears to be slightly shifted (Fig. S5A). To verify if the slightly shifted density indeed can be attributed to H_2O1, we calculated the H-bond distances and energies of the residues that are interacting with this water molecule in the ^{apo}AdiC-wt structure: the carbonyl oxygen of A96 (TM3) and S357 (TM10). Fig. S5B shows the analysis of H-bonds formed by these two residues and water molecules during the course of the MD simulations. Consistent with the observation in the ^{apo}AdiC-wt structure (Fig. 3), S357 forms one hydrogen bond with a water molecule in the region occupied by H_2O1, whereas A96 participates in formation of mostly two H-bonds with water molecules in the regions occupied by H_2O1, H_2O2, or H_2O3. The exchange of water molecules at the crystallographically resolved H_2O1–H_2O4 sites was observed to occur on a nanosecond time-scale indicating convergence of the simulations in this respect, thus rendering the results independent of the initial water placement.

Comparison of Protein–Substrate Interactions in the Arg-Bound AdiC-N22A and ^{Agm}AdiC-wt Structures. Protein-substrate interactions between the previously published outward-facing occluded Arg-bound AdiC-N22A (^{Arg}AdiC-N22A) structure (10) and the outward-open Agm-bound AdiC-wt (^{Agm}AdiC-wt) structure reported herein were compared. In the ^{Arg}AdiC-N22A structure, the negatively charged α-carboxylate group of Arg accepts two H-bonds from the side-chain S26 and the amide nitrogen of G27 (10) (Fig. S6A). Such interactions are missing in the ^{Agm}AdiC-wt structure because Agm lacks the α-carboxylate group (Fig. S6B). For comparison of the substrate-binding pockets and protein–substrate interactions see, in addition to Fig. S6, the stereoview representation of the superpositioned ^{Agm}AdiC-wt and ^{Arg}AdiC-N22A structures in Fig. S7. The positively charged α-amino group of Arg in the ^{Arg}AdiC-N22A structure donates three H-bonds to the carbonyl oxygen atoms of I23 (TM1), and W202 and I205 in TM6 (10) (Fig. S6A). The two substrate interactions with I23 (TM1) and I205 (TM6) persist with the primary amino group of Agm in the ^{Agm}AdiC-wt structure (Fig. S6B). Because of the different conformational states of ^{Arg}AdiC-N22A and ^{Agm}AdiC-wt (i.e., outward-facing occluded and outward-open), the H-bond distances between the primary amino groups of Arg and Agm, and W202 (TM6) differ significantly [i.e., 2.9 Å (^{Arg}AdiC-N22A) and 3.9 Å (^{Agm}AdiC-wt)]; additionally, W202 is responsible for occlusion of substrate from the periplasm. Consequently, this H-bond is basically abolished in the ^{Agm}AdiC-wt structure. An additional amino acid, S203 (TM6), is in H-bond distance to the primary amino group of Arg. The H-bond distance between the carbonyl oxygen atom of S203 (TM6) is increased from 3.1 Å to 3.4 Å in the ^{Agm}AdiC-wt structure compared with the ^{Arg}AdiC-N22A structure. Globally, the distances between the interacting amino acids in the two structures are more favorable for H-bonding in the ^{Arg}AdiC-N22A structure, thus resulting potentially in stronger binding of the primary amino group of the substrate to the protein. In both

structures, the Gdm groups of Arg and Agm stack against W293 (TM8) through cation–π interactions (Figs. S6 and S7). The nitrogen atoms Nη1 and Nη2 of the Arg and Agm Gdm groups in the ^{Arg}AdiC-N22A and ^{Agm}AdiC-wt structures are located within H-bond distance to three oxygen atoms: that is, the oxygen atom of the side-chain N101 (TM3), and the carbonyl oxygen atoms of A96 and C97 in TM3 (Fig. S6). These H-bond distances are shorter in the ^{Agm}AdiC-wt structure compared with the ^{Arg}AdiC-N22A structure, possibly leading to stronger binding of the substrate Gdm group (Fig. S6). An additional, previously described H-bond between Arg and AdiC-N22A is established between the Nη2 nitrogen atom of the Gdm group and the side chain hydroxyl group of S357 (TM10) (10) (Fig. S6A). Interestingly, this interaction is not present in this form in the ^{Agm}AdiC-wt structure. Instead, the interaction of S357 (TM10) with the Gdm group of Agm is bridged by a water molecule (H2O1), involving an additional H-bond contributed by the carbonyl oxygen atom of A96 (TM3) (Fig. S6B). This H-bond network contributes to the binding, positioning, and stabilization of the Gdm group and thus of the Agm molecule in the binding pocket. The aliphatic portion of Arg in the ^{Arg}AdiC-N22A structure interacts with the side chains of the three hydrophobic amino acids W202 and I205 in TM6, and W293 (TM8) (Fig. S3B). Interactions are similar in the ^{Agm}AdiC-wt structure with the exception of W202 (TM6). This interaction of Agm with W202 (TM6) is missing because the ^{Agm}AdiC-wt structure is in the outward-open and not in the outward-facing occluded state as the ^{Arg}AdiC-N22A structure. In general, the described differences between substrate binding in the ^{Agm}AdiC-wt and ^{Arg}AdiC-N22A structures result mainly because of the difference in substrates, a slightly different position of the substrates in the binding pockets (compare substrates in Figs. S6 and S7), and different conformational states of the transporter.

Potential Conformational Changes in AdiC upon Release of Agm. Toward understanding the conformational changes of AdiC involved in the release of Agm into the periplasmic space of *E. coli* (Fig. 1B), we created a morph using the previously published outward-facing occluded ^{Arg}AdiC-N22A (10), and the outward-open ^{Agm}AdiC-wt and ^{apo}AdiC-wt structures presented herein, in

this given order (Movie S1). For the initial conformational state in the morph, Arg in the ^{Arg}AdiC-N22A structure was converted into Agm by removing the carboxylate group in silico (^{Agm}AdiC-N22A) (Fig. S8A). As seen in Fig. S8, Agm is sandwiched between W202 (TM6) and W293 (TM8) in the outward-facing occluded state. About 8 Å away from the substrate-binding site toward the cytoplasm, the amino acids Y93, E208, and Y365 are located, which represent the intracellular (distal) gate (Fig. S8) (10). Under extreme acidic conditions, it was demonstrated by MD simulations that residue E208 is accessible to water from the periplasmic side, allowing its protonation (19). Protonation leads to the abolishment of the attractive electrostatic interaction between E208 and the doubly positively charged Agm molecule. In addition, E208 protonation causes rearrangement of H-bonds at the intracellular (distal) gate (19). The importance of this residue is underlined by the facts that substrate transport is basically abolished in the AdiC-E208A mutant (9), and that this residue is conserved in the three virtual proton pumps from *E. coli* (Fig. S9). Possibly, E208 protonation induces a conformational shift to the outward-open state (^{Agm}AdiC-wt structure), which represents how Agm is released (Movie S1). Thereby, major conformational changes are observed in TM2, TM6, and TM10, from which TM6 undergoes the most pronounced one (Fig. S10). As a consequence, W202 in TM6, which initially interacts with the amino group (via its carbonyl group) and the aliphatic moiety of Agm (via its side chain) (Fig. S8A), swings out, basically breaking these interactions and thus opening the exit pathway for Agm from the binding pocket (Fig. S8B). Importantly, switching to the outward-open conformation facilitates solvation of the substrate-binding site.

An interesting feature of this conformational change and solvation, visualized in the here presented ^{Agm}AdiC-wt structure, is the binding of a water molecule (H2O1) between S357 (TM10) and Nη2 of the Agm Gdm group, which was initially missing (Fig. S8 and Movie S1). Considering the H-bond distances between the hydroxyl group of S357 (TM10) and Nη2 of the Gdm group, and between H2O1 and Nη2 (Fig. S8) (i.e., 3.3 Å and 3.7 Å), protein–substrate interaction gets weakened in the transition
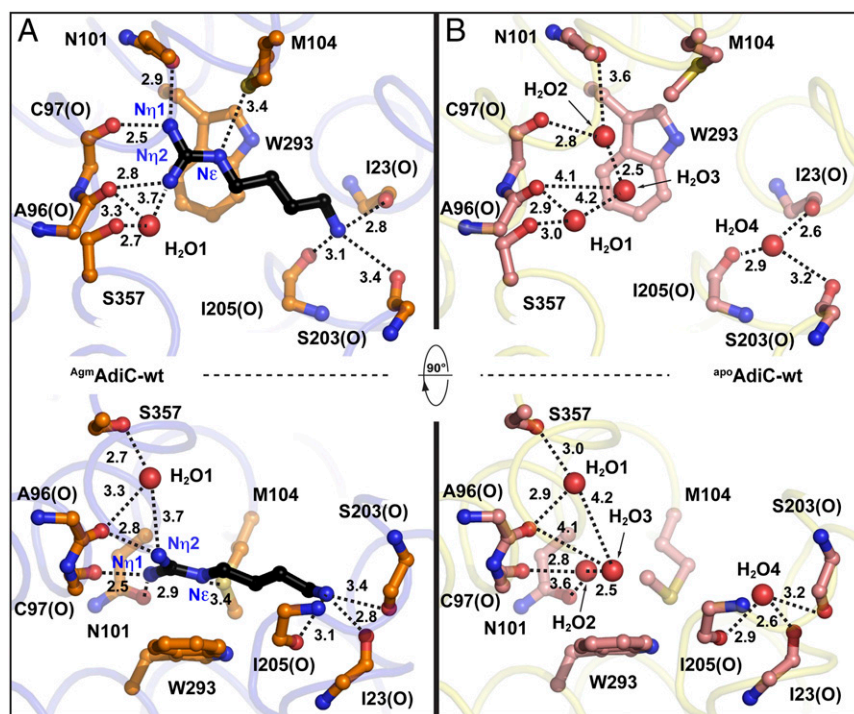
Fig. 3. Comparison of the substrate-binding sites in the Agm-bound and substrate-free AdiC structures. (A) Recognition of the substrate Agm by specific amino acids in AdiC and one protein-associated water molecule (H2O1). Important amino acids are labeled in the one letter code and when interacting with their main-chain carbonyl oxygen atoms additionally labeled with (O). The three Gdm group nitrogen atoms of Agm are labeled Nε, Nη1, and Nη2. The top view from the periplasmic side (*Upper*) and side view (tilted by 90°) from the membrane plane (*Lower*) onto the Agm binding site are displayed. For van der Waals interactions between AdiC and the aliphatic portion of Agm (e.g., with the side chain of I205) see Fig. S3A. (B) Same views and labeling as in A for the substrate-free AdiC structure. The ^{Agm}AdiC-wt (A) and ^{apo}AdiC-wt (B) structures and specific amino acid residues in the substrate-binding pockets are represented as ribbons in blue and yellow, and as sticks in gold and salmon, respectively. Crystallographic water molecules are displayed as red balls, and potential H-bonds and interatomic distances are indicated as dotted lines and in Ångstrom, respectively.

from the outward-facing occluded to the outward-open state by the addition of water, thus further facilitating release of Agm from AdiC. Water molecules from the bulk solution then specifically replace Agm, and the methylmercapto moiety of M104 rotates by ~180° to protrude into the substrate-binding pocket as represented in the [apo]AdiC-wt structure (Fig. 3, Fig. S2, and Movie S1). Finally, Tsai and Miller (6) proposed recently that under extreme acidic conditions protonation of the periplasmic surface of AdiC in the outward-open conformation renders the substrate-binding pocket inhospitable for doubly positively charged molecules such as Agm, thus promoting its unloading into the extracellular space.

Amino Acid Sequence Analysis of the Three Virtual Proton Pumps from *E. coli*. Three virtual proton pumps were described in *E. coli* (20) [i.e., the exchangers AdiC (Arg/Agm), CadB (lysine/cadaverine), and PotE (ornithine/putrescine)], all belonging to the APC superfamily. Imported and exported substrates are amino acids and their decarboxylated forms, respectively. Although the three substrate amino acids possess positively charged side chains, this charge is localized on different chemical groups: a Gdm group (Arg) and a primary amino group (lysine and ornithine). Having identified the crucial amino acid side chains in AdiC involved in Agm binding (Fig. 3), we wondered if these residues are also conserved in CadB and PotE. It should be noted that amino acid residues involved in Agm binding via backbone interactions were not considered because they are exchangeable by most of the proteinogenic amino acids. The above-discussed aromatic residues W202 and W293 in AdiC, which are involved in substrate occlusion to the periplasm and substrate binding, were fully conserved in the other two virtual proton pumps from *E. coli* (Fig. S9). Also fully conserved in CadB and PotE is the AdiC residue N101 (TM3), which forms with the oxygen atom of the amide group a H-bond with Nη1 of the Agm Gdm group (Fig. 3) and E208 (TM6), which is involved in dissociation and release of Agm to the periplasmic space under extreme acidic conditions (19) (Fig. S9). Not conserved in CadB and PotE are the amino acid residues M104 (TM3) and S357 (TM10) of AdiC (Fig. S9). As described above, the sulfur atom of the methylmercapto group of M104 (TM3) serves as hydrogen acceptor for Nε of the Agm Gdm group (Fig. 3). S357 (TM10) is also involved in the binding of the Agm Gdm group, but indirectly via the identified water molecule H_2O1, which interacts with Nη2 (Fig. 3). Thus, both residues, M104 (TM3) and S357 (TM10), interact directly and indirectly with the Gdm of Agm. In CadB and PotE, the AdiC residues M104 (TM3) and S357 (TM10) are replaced by the amino acid residues isoleucine and alanine (Fig. S9), whose side chains preclude interactions with a Gdm group. This finding makes sense because the primary amino groups in the side chains of lysine/cadaverine and ornithine/putrescine contain only one nitrogen atom, which is most obviously represented by Nη1 in the Gdm group of Arg/Agm, and interactions with the additional two nitrogen atoms Nη2 and Nε of the Gdm group are not necessary for substrate recognition and binding.

Ligand Binding Affinity of AdiC-wt and Selected Mutants. The binding affinities of AdiC-wt for the substrates Arg and Agm were determined by SPA. AdiC-wt has with 148 μM (Arg) and 56 μM (Agm) (Table 1; see Fig. S1 for raw data) an about threefold higher affinity for Agm compared with Arg. In addition, we determined the affinities of the previously reported mutants AdiC-N22A (10) and AdiC-S26A (6) for Arg and Agm (Table 1; see Fig. S1 for raw data). AdiC-N22A showed an about sixfold higher affinity for Arg and, interestingly, an about fourfold lower affinity for Agm compared with AdiC-wt (Table 1). Thus, the mutation N22A in AdiC results in an inversion of the specificities of the substrates compared with AdiC-wt (Table 1). The affinity of

AdiC-S26A for Arg was comparable to that of AdiC-wt, whereas that for Agm was about 1.5-fold lower, but still higher than for Arg (Table 1). Consequently, this mutation does not have a significant effect and only a weak effect on the affinities of AdiC-S26A for Arg and Agm compared with AdiC-wt. The affinities of AdiC-wt, AdiC-N22A and AdiC-S26A for the Arg analogs: L-arginine methyl ester (Arg-OMe) and L-arginine amide (Arg-NH$_2$) were also determined by SPA (Table 1; see Fig. S1 for raw data). AdiC-N22A had with 77 μM the highest affinity for Arg-OMe, followed by AdiC-wt with 293 μM and AdiC-S26A with 1,693 μM. Hence, absence of the negative charge in Arg-OMe compared with Arg induces a loss in affinity of about 3.5-fold in AdiC-N22A and of about twofold in AdiC-wt for Arg-OMe. Strikingly, AdiC-S26A had a dramatically lower affinity for Arg-OMe compared with AdiC-N22A and AdiC-wt, indicating the high importance of S26 for Arg-OMe binding. Considering that AdiC-wt and AdiC-S26A have similar binding affinities for Arg, but huge differences for Arg-OMe, different ligand binding mechanisms are expected for Arg and Arg-OMe. Based on these results, we wondered about the role of S26 in AdiC-N22A in Arg binding, and introduced the additional mutation S26A. Strikingly, the AdiC-N22A-S26A double mutant was only able to bind [³H]Arg to similar levels as AdiC-N101A and -W293A (Fig. S4A). As mentioned above, mutations at these two positions give rise to AdiC versions with dramatically decreased and mostly even completely abolished binding and transport function (2, 8, 11). The SPA result with AdiC-N22A-S26A is unexpected considering the irrelevance of S26 in AdiC-wt for Arg binding (Table 1). Arg-NH$_2$ was previously used as an isosteric proxy for protonated Arg^{2+} (8, 21). All three AdiC forms had low affinities for Arg-NH$_2$ (Table 1).

Discussion

Toward understanding of the molecular working mechanisms of the Arg/Agm antiporter AdiC and members of the APC superfamily, we have provided the structure of the wild-type form of AdiC with bound Agm at 2.6-Å resolution. The [Agm]AdiC-wt structure allowed the description of Agm binding to AdiC at the molecular level (Fig. 3A) and currently represents the only structure of AdiC-wt with a bound substrate. Furthermore, the structure of substrate-free AdiC-wt was determined at the unprecedented resolution of 2.2 Å. Both high-resolution structures made possible the identification of crucial water molecules, and protein-water and Agm-water H-bond networks in the AdiC substrate-binding pockets (Fig. 3). Importantly, positions of specific nitrogen atoms of the Agm molecule in the [Agm]AdiC-wt structure were found to be replaced by water molecules in the [apo]AdiC-wt structure, thus preserving to a high extent the structure of the substrate-binding pocket in the absence of substrate. Fang et al. (3) showed by isothermal titration calorimetry (ITC) that Arg and Agm binding to AdiC is enthalpically unfavorable and therefore entropy-driven. Considering the presence of bound water molecules in the [apo]AdiC-wt structure, which have lower entropy compared with water molecules in the bulk solution, binding of Arg and Agm to AdiC will cause their release. This process leads to an increase in entropy favoring substrate binding and is in line with the results from ITC (3). Comparison of the published outward-facing occluded [Arg]AdiC-N22A structure (10) with the outward-open [Agm]AdiC-wt structure led to the identification of an additional role of water in the substrate-binding pocket. As illustrated in Fig. S6 and described in *Results*, S357 makes a direct contact to the substrate in the outward-facing occluded state, whereas in the outward-open state interaction of the substrate to the protein is bridged by a water molecule (H_2O1 in Fig. S6; see also Fig. S7 for a stereoview representation), thus weakening this interaction. Furthermore, this water molecule is involved in the stabilization of TM3 and TM10 in the outward-open [apo]AdiC-wt and [Agm]AdiC-wt structures, which is not the case and sterically impossible in this form in the outward-facing occluded [Arg]AdiC-N22A structure (Fig. S6).

The current view on the release of Agm from AdiC into the periplasm (Fig. 1B) considering the involvement of water molecules was visualized in a morph (Movie S1) and described in *Results*. The existence of bound water molecules, and thus of their possible functional implications, in AdiC was supported by MD simulations performed at human body core temperature at which pathogenic bacteria act. The [Agm]AdiC-wt structure allowed a comparison with the [Arg]AdiC-N22A structure, and thus of the molecular interactions involved in Arg and Agm binding (Fig. S6). Importantly, comparison of these two substrate bound structures that are in different conformational states (outward-open, Agm-bound and outward-facing occluded Arg-bound) identified differences critical for substrate binding (Fig. S6). The AdiC mutant N22A was shown to have an approximately sixfold higher affinity for Arg compared with AdiC-wt as determined by ITC (10). We obtained similar results using the SPA (Table 1), in agreement with the previously published results (10). The affinity of AdiC-N22A for Agm was not previously addressed. Therefore, we determined using the SPA the affinity of AdiC-N22A for Agm, which was almost 10-fold lower compared with Arg (Table 1). A higher affinity for Arg compared with Agm is an unexpected result, which indicates an inversion of the specificity of AdiC-N22A for these two substrates compared with AdiC-wt (Table 1) and thus an artificial situation. The binding affinities of AdiC-wt, AdiC-N22A, and AdiC-S26A for Arg, Agm, Arg-OMe, and Arg-NH₂ determined by SPA were not comparable, indicating significantly different ligand–protein interactions between the different AdiC forms. As an exception, the K_is of AdiC-wt and AdiC-S26A for Arg were comparable (Table 1). The two Arg-bound crystal structures of AdiC-N22A (10) and AdiC-N101A (11) revealed hydrogen bonding between the α-carboxyl group of Arg and the hydroxyl group of S26. From such a configuration, a substrate-recognition mechanism would naturally be deduced. However, based on our SPA results (Table

1) the binding affinities of AdiC-wt and AdiC-S26A for Arg are similar, indicating no significant contribution of S26 in binding of the substrate Arg. These results are supported by recent uptake experiments with AdiC-S26A, which indicate that this AdiC mutant is fully transport competent (6). Thus, inversion of the Arg and Agm specificity of AdiC-N22A compared with AdiC-wt, the mostly different ligand binding affinities for AdiC-wt, AdiC-N22A, and AdiC-S26A, and the unimportance of S26 in AdiC-wt for Arg binding compared with AdiC-N22A (Table 1) raise the critical question of to which extent structures of mutant AdiC reflect the physiological substrate binding mechanism in wild-type AdiC. Therefore, the high-resolution structures presented herein provide the most accurate and reliable views on the architecture and protein–substrate interactions of the naturally occurring wild-type AdiC protein currently available. Finally, because of their high resolutions, both AdiC-wt structures provide a solid basis for future homology modeling studies of APC family members to understand their working mechanisms at the molecular level and for structure-based drug design as exemplified by the recent work with human LAT1 (13).

Methods

AdiC was cloned, overexpressed and purified as described previously (22). SPA experiments using purified AdiC were performed according to ref. 16. For details, see *SI Methods*. Crystallization, structure determination and molecular dynamics simulations were conducted as described in *SI Methods*.

1. Foster JW (2004) *Escherichia coli* acid resistance: Tales of an amateur acidophile. *Nat Rev Microbiol* 2(11):898–907.
2. Casagrande F, et al. (2008) Projection structure of a member of the amino acid/polyamine/organocation transporter superfamily. *J Biol Chem* 283(48):33240–33248.
3. Fang Y, Kolmakova-Partensky L, Miller C (2007) A bacterial arginine-agmatine exchange transporter involved in extreme acid resistance. *J Biol Chem* 282(1):176–182.
4. Gong S, Richard H, Foster JW (2003) YjdE (AdiC) is the arginine:agmatine antiporter essential for arginine-dependent acid resistance in *Escherichia coli*. *J Bacteriol* 185(15):4402–4409.
5. Iyer R, Williams C, Miller C (2003) Arginine-agmatine antiporter in extreme acid resistance in *Escherichia coli*. *J Bacteriol* 185(22):6556–6561.
6. Tsai MF, Miller C (2013) Substrate selectivity in arginine-dependent acid resistance in enteric bacteria. *Proc Natl Acad Sci USA* 110(15):5893–5897.
7. Wang S, Yan R, Zhang X, Chu Q, Shi Y (2014) Molecular mechanism of pH-dependent substrate transport by an arginine-agmatine antiporter. *Proc Natl Acad Sci USA* 111(35):12734–12739.
8. Fang Y (2009) Structure of a prokaryotic virtual proton pump at 3.2 Å resolution. *Nature* 460(7258):1040–1043.
9. Gao X, et al. (2009) Structure and mechanism of an amino acid antiporter. *Science* 324(5934):1565–1568.
10. Gao X, et al. (2010) Mechanism of substrate recognition and transport by an amino acid antiporter. *Nature* 463(7282):828–832.
11. Kowalczyk L, et al. (2011) Molecular basis of substrate-induced permeation by an amino acid antiporter. *Proc Natl Acad Sci USA* 108(10):3935–3940.
12. Fotiadis D, Kanai Y, Palacín M (2013) The SLC3 and SLC7 families of amino acid transporters. *Mol Aspects Med* 34(2-3):139–158.
13. Geier EG, et al. (2013) Structure-based ligand discovery for the large-neutral amino acid transporter 1, LAT-1. *Proc Natl Acad Sci USA* 110(14):5480–5485.
14. Rosell A, et al. (2014) Structural bases for the interaction and stabilization of the human amino acid transporter LAT2 with its ancillary protein 4F2hc. *Proc Natl Acad Sci USA* 111(8):2966–2971.
15. Hinz KM, et al. (2015) Structural insights into thyroid hormone transport mechanisms of the L-type amino acid transporter 2. *Mol Endocrinol* 29(6):933–942.
16. Harder D, Fotiadis D (2012) Measuring substrate binding and affinity of purified membrane transport proteins using the scintillation proximity assay. *Nat Protoc* 7(9):1569–1578.
17. Zhou P, Tian F, Lv F, Shang Z (2009) Geometric characteristics of hydrogen bonds involving sulfur atoms in proteins. *Proteins* 76(1):151–163.
18. Biswal HS, Gloaguen E, Loquais Y, Tardivel B, Mons M (2012) Strength of NH···S hydrogen bonds in methionine residues revealed by gas-phase IR/UV spectroscopy. *J Phys Chem Lett* 3(6):755–759.
19. Zomot E, Bahar I (2011) Protonation of glutamate 208 induces the release of agmatine in an outward-facing conformation of an arginine/agmatine antiporter. *J Biol Chem* 286(22):19693–19701.
20. Tomitori H, Kashiwagi K, Igarashi K (2012) Structure and function of polyamine-amino acid antiporters CadB and PotE in *Escherichia coli*. *Amino Acids* 42(2-3):733–740.
21. Tsai MF, Fang Y, Miller C (2012) Sided functions of an arginine-agmatine antiporter oriented in liposomes. *Biochemistry* 51(8):1577–1585.
22. Ilgü H, et al. (2014) Variation of the detergent-binding capacity and phospholipid content of membrane proteins when purified in different detergents. *Biophys J* 106(8):1660–1670.
23. Kabsch W (2010) XDS. *Acta Crystallogr D Biol Crystallogr* 66(Pt 2):125–132.
24. Adams PD, et al. (2010) PHENIX: A comprehensive Python-based system for macromolecular structure solution. *Acta Crystallogr D Biol Crystallogr* 66(Pt 2):213–221.
25. Emsley P, Lohkamp B, Scott WG, Cowtan K (2010) Features and development of Coot. *Acta Crystallogr D Biol Crystallogr* 66(Pt 4):486–501.
26. Wolf MG, Hoefling M, Aponte-Santamaría C, Grubmüller H, Groenhof G (2010) g_membed: Efficient insertion of a membrane protein into an equilibrated lipid bilayer with minimal perturbation. *J Comput Chem* 31(11):2169–2174.
27. Berendsen H, Grigera J, Straatsma T (1987) The missing term in effective pair potentials. *J Phys Chem* 91(24):6269–6271.
28. Lindorff-Larsen K, et al. (2010) Improved side-chain torsion potentials for the Amber ff99SB protein force field. *Proteins* 78(8):1950–1958.
29. Berger O, Edholm O, Jähnig F (1997) Molecular dynamics simulations of a fluid bilayer of dipalmitoylphosphatidylcholine at full hydration, constant pressure, and constant temperature. *Biophys J* 72(5):2002–2013.
30. Bussi G, Donadio D, Parrinello M (2007) Canonical sampling through velocity rescaling. *J Chem Phys* 126(1):014101.
31. Parrinello M, Rahman A (1981) Polymorphic transitions in single crystals: A new molecular dynamics method. *J Appl Phys* 52(12):7182–7190.
32. Essmann U, et al. (1995) A smooth particle mesh Ewald method. *J Chem Phys* 103(19):8577–8593.
33. Espinosa E, Molins E, Lecomte C (1998) Hydrogen bond strengths revealed by topological analyses of experimentally observed electron densities. *Chem Phys Lett* 285(3):170–173.
34. Aponte-Santamaría C, Briones R, Schenk AD, Walz T, de Groot BL (2012) Molecular driving forces defining lipid positions around aquaporin-0. *Proc Natl Acad Sci USA* 109(25):9887–9892.

BIOPHYSICS AND COMPUTATIONAL BIOLOGY

Supporting Information

SI Methods

Cloning of AdiC. The gene of AdiC was cloned from genomic DNA of *Escherichia coli* XL1-Blue by PCR using the forward primer 5′ AAAA AAGCTT ATG TCT TCG GAT GCT GAT GCTC 3′ and the reverse primer 5′ AAAA CTCGAG ATC TTT GCT TAT TGG TGC ATC 3′. The PCR products were digested with the restriction enzymes HindIII and XhoI, and ligated into the pZUDF21 vector (22). The DNA constructs were verified by sequencing. The pZUDF21–AdiC construct results in a recombinant AdiC protein with a human rhinovirus 3C (HRV3C) protease cleavage site followed by a deca-His tag at the C terminus. The calculated molecular mass of the recombinant and cleaved monomeric AdiC is ~49.5 kDa.

Protein Preparation. For overexpression, pZUDF21–AdiC was transformed into BL21(DE3) pLysS *E. coli* cells. The cells were allowed to grow in Luria Bertani (LB) medium supplemented with 0.1 mg/mL ampicillin at 37 °C by shaking in an orbital shaker. Protein expression was induced at OD_{600} of 0.5–0.6 with 0.3 mM isopropyl-β-D-thiogalactopyranoside and incubated at 37 °C for 3 h. Cells were then harvested by centrifugation ($10,000 \times g$ for 10 min at 4 °C), resuspended in Lysis buffer (20 mM Tris·HCl pH 8.0, 500 mM NaCl) supplemented with 5 mM EDTA, and stored at −20 °C until further use. For membrane preparation, frozen cells were thawed and lysed using a Microfluidizer M-110P (Microfluidics) at 16,000 psi (four passages). Cell debris were removed by centrifugation ($12,000 \times g$ for 20 min at 4 °C) and from the supernatant, membranes were collected by ultracentrifugation ($150,000 \times g$ for 1 h at 4 °C). The pellet was homogenized in Lysis buffer supplemented with 5 mM EDTA and an additional ultracentrifugation was performed. The pellet was then homogenized in a small volume of Lysis buffer (12-mL final volume for membranes from 8-L cell culture) and aliquoted into fractions corresponding to membranes from 1 L of cell culture. Membrane aliquots were frozen in liquid nitrogen and stored at −80 °C until further use.

Purification of AdiC. For purification, one aliquot of membrane suspension was solubilized for 2 h at 4 °C on a rotational shaker in 20 mM Tris·HCl pH 8.0, 300 mM NaCl, 10% (vol/vol) glycerol, 4% (wt/vol) *n*-nonyl-β-D-glucopyranoside (NG) ($V_{tot} = 7$ mL). After ultracentrifugation ($100,000 \times g$ for 1 h at 4 °C), the supernatant was diluted twofold in 20 mM Tris·HCl pH 8.0, 300 mM NaCl, 10% (vol/vol) glycerol, 0.4% (wt/vol) NG (Buffer A) containing 5 mM L-histidine and incubated with 0.5 mL (bed volume) pre-equilibrated Ni-NTA Superflow resin (Qiagen) for 2 h at 4 °C on a rotational shaker (metal affinity chromatography). The resin was then transferred into a column and washed three times with 5 mL of Buffer A containing 5 mM L-histidine and 3 mL of Buffer A by gravity flow. The His-tag on AdiC was removed by on-column cleavage on a rotational shaker for 18 h at 4 °C by addition of 200 µg of human rhinovirus 3C protease (HRV3C; BioVision). Finally, the cleaved AdiC was eluted by centrifugation ($3,000 \times g$ for 15 s at 4 °C) and remaining HRV3C was removed by an additional incubation of the eluate with 100 µL (bed volume) pre-equilibrated Ni-NTA Superflow resin followed by a subsequent filtration to remove the resin. All detergents used in this study were obtained from Glycon Biochemicals.

Crystallization of AdiC. For crystallization, the purified protein was concentrated to about 17 mg/mL using a 50-kDa Amicon cut-off filter (Sigma-Aldrich) and ultracentrifuged ($200,000 \times g$ for 30 min at 4 °C) before use. Initial search for crystallization hits was performed using a Mosquito nanoliter crystallization robot (TTP Labtech) and the MemGold sparse matrix screening kit (Molecular Dimensions). After several screening rounds, 100- to 200-µm crystals appeared after 5–7 d in sitting-drop vapor-diffusion plates at a 1:1 drop ratio. The crystallization solution of the crystals contained 62.5 mM Tris·HCl pH 8.0, 35% (vol/vol) PEG400, and 1% (wt/vol) NG. For cocrystallization of AdiC with agmatine, 2 mM agmatine was added to the protein solution before crystallization using the same condition as described before. Crystals were collected, flash-frozen and stored in liquid nitrogen until X-ray analysis.

Structure Determination. All native datasets of AdiC (that is, with and without agmatine molecule) were collected on frozen crystals at the X06SA (PXI) beamline of the Swiss Light Source (SLS; Paul Scherrer Institute, Villigen, Switzerland) using a PILATUS 6M detector. Diffraction data were processed with XDS (23). The structure of substrate-free wild-type AdiC (^{apo}AdiC-wt) was determined by molecular replacement with Phaser in Phenix (24) using the coordinates of the AdiC structure with the PDB ID code 3OB6 (11). Default parameters in phenix.refine including Translation/Libration/Screw (TLS) parameters (eight defined groups per AdiC monomer) were used for refinement. The model was improved by carrying out iterative cycles of phenix.refine (24) and manual model building in Coot (25). The Agm-bound wild-type AdiC (^{agm}AdiC-wt) structure was determined as described above using the coordinates of ^{apo}AdiC-wt and without TLS parameters for refinement. The agmatine molecule was placed in a clear density located in the substrate binding pocket and further refined. Figures were generated with PyMOL (www.pymol.org). Data collection and refinement statistics are listed in Table S1.

MD Simulation. The ^{apo}AdiC-wt structure was embedded into a 1-palmitoyl-2-oleoylphosphatidylcholine bilayer using g_membed (26). The crystallographic water positions were retained and additional water molecules were placed by means of the software Dowser (danger.med.unc.edu/hermans/dowser/dowser.htm). Subsequently, the simulation box was solvated using the Gromacs tool genbox with an SPC/E water model (27), and Na^+ and Cl^- ions were added to neutralize the system and reach a salt concentration of 150 mM. The Amber99SB*-ILDN (28) force field was used for simulations with the lipid parameters from Berger et al. (29). Ten independent MD simulations of 100-ns each were performed starting from an energy-minimized system. The temperature during the simulations was kept at 310 K by means of the velocity rescaling thermostat (30) with a time constant of 0.1 ps. The pressure was coupled semi-isotropically to 1 bar reference using the Parrinelo-Rahman barostat (31) with a time constant of 5 ps. Particle-mesh Ewald (32) was used to treat electrostatic interactions. Cut-off values for the short range electrostatic and van der Waals interactions were set to 1 nm. GROMACS 5.0 (www.gromacs.org) was used to carry out the simulations and process the generated trajectories. Hydrogen bond energies were estimated using the Espinosa et al. equation (33). Water densities were calculated as previously described (34) and analyzed separately for both AdiC monomers.

K_i Determination and Binding Assay. Inhibition constants were determined by applying the SPA (16). Briefly, AdiC was solubilized and purified as described above using *n*-dodecyl-β-D-maltopyranoside (DDM): 1.5% (wt/vol) for solubilization and

0.04% (wt/vol) for purification. The AdiC protein was eluted from the Ni-NTA column with 20 mM Tris·HCl, pH 8.0, 300 mM NaCl, 10% (vol/vol) glycerol, 0.04% (wt/vol) DDM, 400 mM imidazole. Imidazole was removed using Zeba Spin Desalting Columns (Thermo Scientific). The competitive inhibition of L-[^{3}H]arginine binding to AdiC was determined by increasing concentrations (e.g., 0, 0.000128, 0.00064, 0.0032, 0.016, 0.8, 4, 20 mM and 100 mM) of Arg, Agm, Arg-OMe, and Arg-NH$_2$ in 50 mM Tris·HCl pH 8.0, 150 mM NaCl, 0.1% (wt/vol) DDM, 1 mM Tris(2-carboxyethyl)phosphine, 10% (vol/vol) glycerol. For the reaction, 2 μg of protein, 1 μCi L-[^{3}H]arginine (specific activity: 40 Ci/mmol; Perkin-Elmer) and 500 μg PVT-copper beads (Perkin-Elmer) in a final volume of 100 μL were incubated per well in 96-well plates (white OptiPlates, Perkin-Elmer). After incubation for 18 h at 4 °C in the dark, samples were counted for 1.5 min with a Packard TopCount (Perkin-Elmer) scintillation counter at 18 °C. Nonspecific signals were determined by adding imidazole to each well to a final concentration of 100 mM followed by overnight incubation before measurement. Nonspecific signals were subtracted from data points. For more information and details on the protocol and optimization of the

SPA for AdiC, see ref. (16). K_i values were calculated by non-linear curve fit using the "one site – Fit K_i" Equation in Prism5 (GraphPad Software).

L-[^{3}H]arginine binding experiments with AdiC-wt, AdiC-N101A, AdiC-W293A, and AdiC-N22A-S26A (Fig. S4*A*) by SPA were performed similarly to the K_i determination assay described above, but in the absence of competitor.

Morph of Conformational Changes in AdiC. Conformational changes involved in Agm release into the periplasmic space of *E. coli* (Fig. 1*B*) were morphed using the previously published outward-facing occluded Arg-bound AdiC-N22A structure ([Arg]AdiC-N22A) (10) (PDB ID code 3L1L), and the here presented [Agm]AdiC-wt and [apo]AdiC-wt structures (Movie S1). The [Arg]AdiC-N22A structure was converted into an Agm-bound structure ([Agm]AdiC-N22A) by removing the α-carboxylate group of Arg with COOT (25). The three structures [Agm]AdiC-N22A, [Agm]AdiC-wt and [apo]AdiC-wt were superpositioned, and the morph of the three structures, in this given order, generated using the University of California, San Francisco Chimera package (www.cgl.ucsf.edu/chimera/).
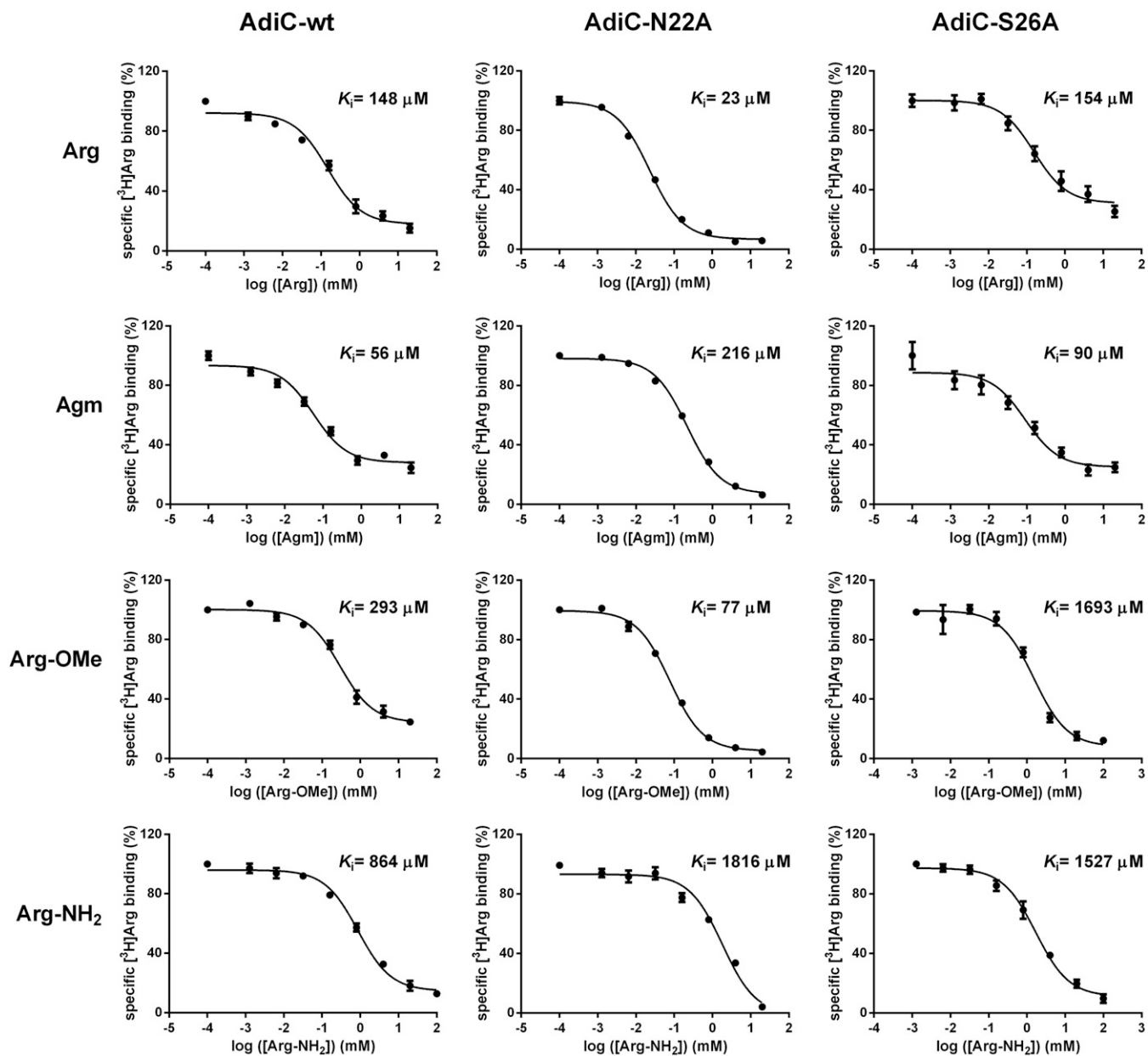
Fig. S1. Ligand-binding affinities determined by SPA of AdiC-wt, AdiC-N22A, and AdiC-S26A. Radioligand: L-[³H]arginine ([³H]Arg). Ligands: L-arginine (Arg), agmatine (Agm), L-arginine methyl ester (Arg-OMe) and L-arginine amide (Arg-NH₂). K_i: inhibition constant (binding affinity). The determined K_i values are from at least three independent experiments, each in triplicate. Error bars represent SEM. For 95% confidence interval values of the corresponding experiments, see Table 1.

Fig. S2. Electron density maps of the [Agm]AdiC-wt (*A*) and [apo]AdiC-wt (*B*) substrate-binding pockets. For example, electron densities of Agm, water molecules and the different rotamer conformations defining M104 (TM3) are discerned. The $2F_o$-F_c electron density maps are contoured at 1.0 σ and colored in magenta ([Agm]AdiC-wt, *A*) and blue ([apo]AdiC-wt, *B*). The [Agm]AdiC-wt and [apo]AdiC-wt structures, and specific amino acid residues in the substrate-binding pockets are represented as ribbons in blue and yellow, and as sticks in gold and salmon, respectively.

Fig. S3. Comparison of the van der Waals interactions between protein and aliphatic portion of the substrates in the [Agm]AdiC-wt and [Arg]AdiC-N22A structures. (*A*) Amino acid residues of [Agm]AdiC-wt involved in van der Waals interactions with the substrate Agm are displayed and labeled in the one letter code. In the *Upper* part of the figure, a top view from the periplasmic side is shown whereas in the lower part a 90° tilted view is displayed. (*B*) For the [Arg]AdiC-N22A structure, same views and labeling as in *A* are shown. The [Agm]AdiC-wt (*A*) and [Arg]AdiC-N22A (*B*) structures, and specific amino acids are represented as ribbons in blue and magenta, and as sticks in gold and light-blue, respectively. The substrates are displayed as black (Agm) and yellow (Arg) sticks, and potential interatomic interactions and their distances are indicated as dotted lines and in Å, respectively.

Fig. S4. Effect of alanine substitution on substrate binding to AdiC determined by SPA. (*A*) Relative comparison of L-[^{3}H]arginine binding to AdiC-wt and selected AdiC mutants. (*B*) Arg and Agm binding affinities of selected AdiC mutants. Radioligand: L-[^{3}H]arginine ([^{3}H]Arg). Ligands: L-arginine (Arg) and agmatine (Agm). K_i: inhibition constant (binding affinity). [^{3}H]Arg binding (*A*) and the determined K_i values (*B*) are from at least three independent experiments, each in triplicate. Error bars represent SEM. For 95% confidence interval values of the affinities determined in *B*, see Table 1.

Fig. S5. MD simulations of ^{apo}AdiC-wt. (*A*) Water densities observed in the MD simulations of both monomers of the ^{apo}AdiC-wt dimer are depicted. The density profiles are consistent for both monomers and are represented at a contour level of 1.0 σ. The crystallographically resolved water positions H_2O1-H_2O4 are displayed as red balls. (*B*) Analysis of hydrogen bonds (H-Bonds) formed by the A96 (TM3) and S357 (TM10) amino acids with water molecules averaged over ten molecular dynamics simulations of 100 ns each of ^{apo}AdiC-wt: number of H-bonds (*Left*), H-bond energies (*Right*). Error bars represent SEM.

Fig. S6. Comparison of the substrate-binding sites of the Arg-bound AdiC-N22A and the Agm-bound AdiC-wt structures. (*A*) Recognition of the substrate Arg by specific amino acids of AdiC-N22A. Amino acids interacting with the substrate are labeled in the one letter code and if the main-chain carbonyl oxygen atom or amide nitrogen are involved additionally labeled with (O) or (N). In the *Upper* part of the panel a top view from the periplasmic side is shown, whereas in the *Lower* part a 90° tilted view is displayed. (*B*) For the [Agm]AdiC-wt structure same views and labeling as in *A* are shown. The [Arg]AdiC-N22A (*A*) and [Agm]AdiC-wt (*B*) structures, and specific amino acids in the substrate-binding pockets, are represented as ribbons in magenta and blue, and as sticks in light-blue and gold, respectively. The substrates are displayed as yellow (Arg) and black (Agm) sticks and the crystallographic water molecule (H$_2$O1) found in the [Agm]AdiC-wt substrate-binding pocket is represented as red ball. Potential H-bonds and interatomic distances are indicated as dotted lines and in Ångstroms, respectively.
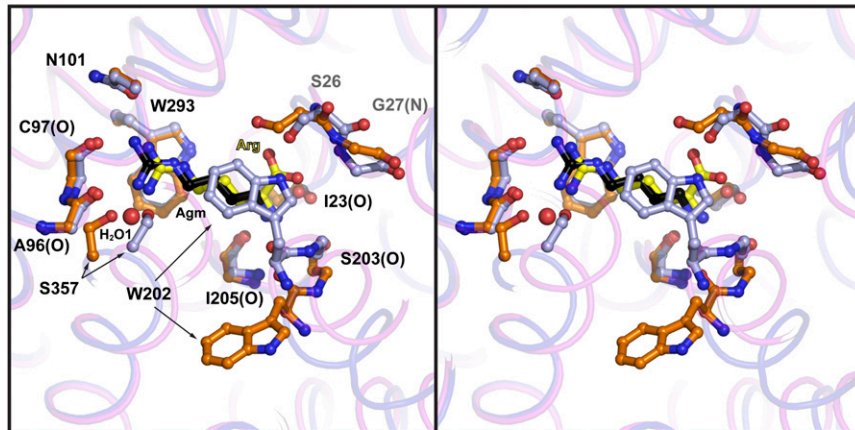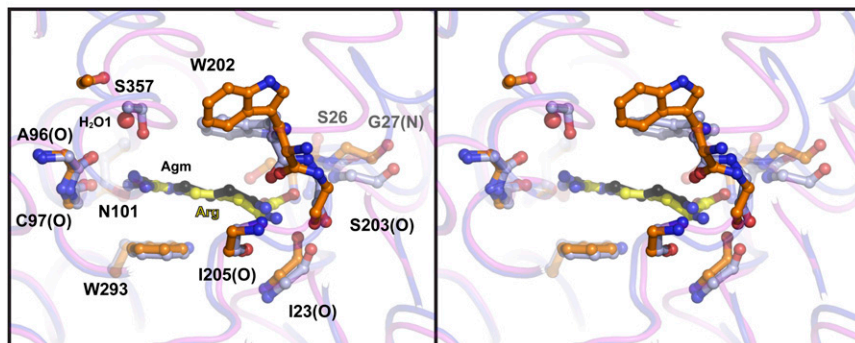
Fig. S7. Superposition and stereoview representation of the substrate-binding sites of the [Arg]AdiC-N22A and the [Agm]AdiC-wt structures. Amino acids interacting with the substrates are labeled in the one letter code and if the main-chain carbonyl oxygen atom or amide nitrogen are involved additionally labeled with (O) or (N). Views from the periplasmic side (*A*) and membrane plane (*B*). The [Arg]AdiC-N22A and [Agm]AdiC-wt structures, and specific amino acids in the substrate-binding pockets, are represented as ribbons in magenta and blue, and as sticks in light-blue and gold, respectively. The substrates are displayed as yellow (Arg) and black (Agm) sticks and the crystallographic water molecule (H$_2$O1) found in the [Agm]AdiC-wt substrate-binding pocket is represented as red ball.
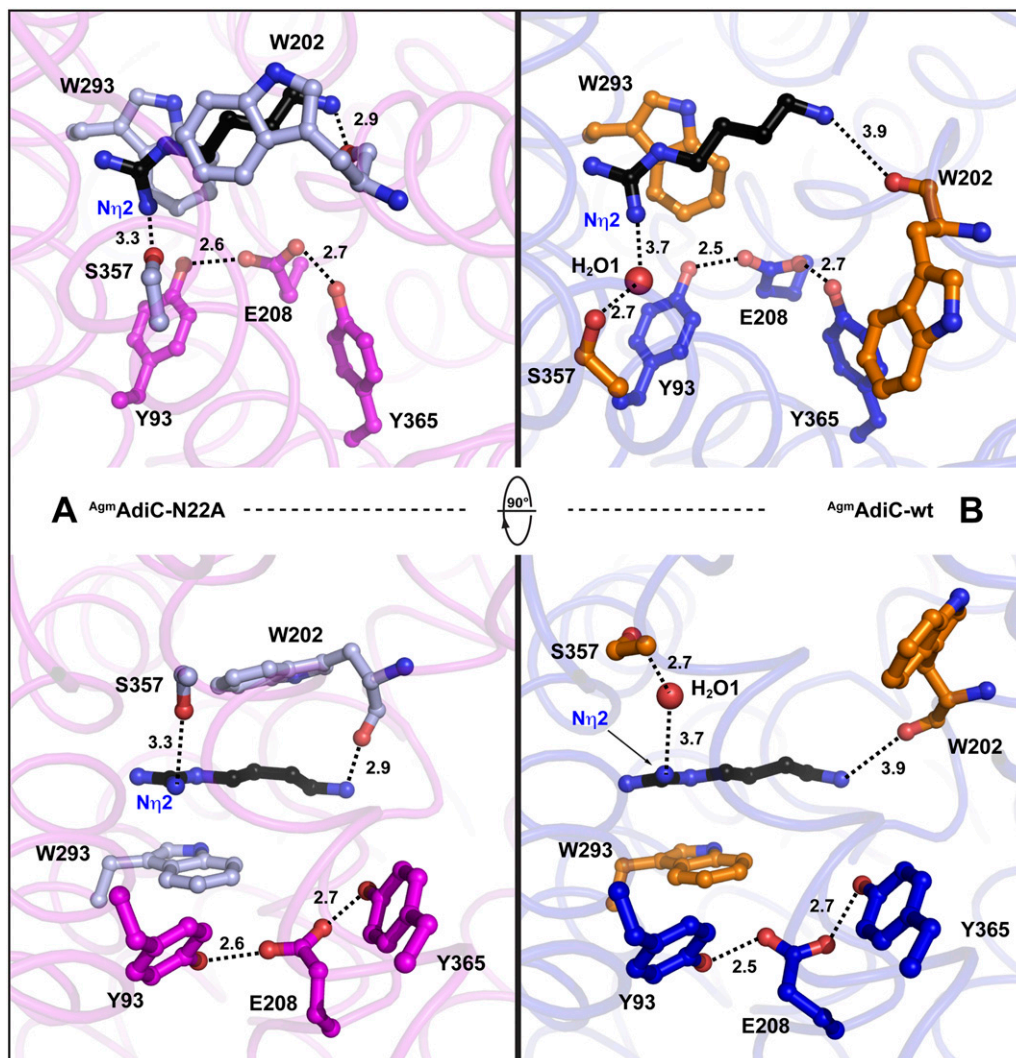
Fig. S8. Comparison of selected amino acids located at the substrate-binding site and the intracellular (distal) gate of Agm-bound AdiC in the outward-facing occluded (*A*; [Agm]AdiC-N22A) and outward-open conformation (*B*; [Agm]AdiC-wt). The former was generated from the published [Arg]AdiC-N22A structure (PDB ID code 3L1L) (10) by removing in silico the carboxylate group from the substrate Arg to obtain Agm. Specific amino acids are labeled in the one letter code. In the *Upper* part of the panel a top view from the periplasmic side is shown whereas in the *Lower* part a 90° tilted view is displayed (view from the membrane plane). (*B*) For the [Agm]AdiC-wt structure the same views and labeling as in *A* are shown. The [Agm]AdiC-N22A (*A*) and [Agm]AdiC-wt (*B*) structures, specific amino acids directly interacting with Agm, and amino acids belonging to the intracellular gate are represented as ribbons in transparent magenta and transparent blue, as sticks in light-blue and gold, and as sticks in magenta and blue, respectively. Agm is displayed as black sticks and the crystallographic water molecule (H_2O1) found in the [Agm]AdiC-wt substrate-binding pocket is represented as red ball. Potential H-bonds and interatomic distances are indicated as dotted lines and in Ångstroms, respectively.

```
AdiC|P60061|   MSSDADAHKVGLIPVTLMVSGNIMGSGVFLLPANLASTGGIAIYGWLVTIIGALGLSMVY    60
CadB|P0AAE8|   ---MSSAKKIGLFACTGVVAGNMMGSGIALLPANLASIGGIAIWGWIISIIGAMSLAYVY    57
PotE|P0AAF1|   -MSQAKSNKMGVVQLTILTMVNMMGSGIIMLPTKLAEVGTISIISWLVTAVGSMALAWAF    59
               :.:.*:*:.  *  :.  *:****: :**::**. *  *:*  .*::: :*::.*:  .:

AdiC|P60061|   AKMSFLDPSPGGSYAYARRCFGPFLGYQTNVLYWLACWIGNIAMVVIGVGYLSYFFPILK   120
CadB|P0AAE8|   ARLATKNPQQGGPIAYAGE-ISPAFGFQTGVLYYHANWIGNLAIGITAVSYLSTFFPVLN   116
PotE|P0AAF1|   AKCGMFSRKSGGMGGYAEYAFGKSGNFMANYTYGVSLLIANVAIAISAVGYGTELLGASL   119
               *: .  . . ** . ** . *:.    :: *   : *.*:**: : .*.* .*   

AdiC|P60061|   DPLVLTITCVVVLWIFVLLNIVGPKMITRVQAVATVLALIPIVGIAVFGWFWFRGETYMA   180
CadB|P0AAE8|   DPVPAGIACIAIVWVFTFVNMLGGTWVSRLTTIGLVLVLIPVVMTAIVGWHWFDAATYAA   176
PotE|P0AAF1|   SPVQIGLATIGVLWICTVANFGGARITGQISSITVWGVIIPVVGLCIIGWFWFSPTLYVD   179
               .*:  ::  :: : ::*:  ..  *: *   ::  ::   .:**:*  .:.**.** 

AdiC|P60061|   AWNVSGLGTFGAIQSTLNVTLWSFIGVESASVAAGVVKNPKRNVPIATIGGVLIAAVCYV   240
CadB|P0AAE8|   NWNTADTTDGHAIIKSILLCLWAFVGVESAAVSTGMVKNPKRTVPLATMLGTGLAGIVYI   236
PotE|P0AAF1|   SWNPHHAPFFSAVGSSIAMTLWAFLGLESACANTDVVENPERNVPIAVLGGTLGAAVIYI   239
                **          *: .:: : **:*:*:***..  : :*:**:*.**:*.: *.  *.: *:

AdiC|P60061|   LSTTAIMGMIPNAALRVSASPFGDAARMALGDTAGAIVSFCAAAGCLGSLGGWTLLAGQT   300
CadB|P0AAE8|   AATQVLSGMYPSSVMAASGAPFAISASTILGNWAAPLVSAFTAFACLTSLGSWMMLVGQA   296
PotE|P0AAF1|   VSTNVIAGIVPNMELANSTAPFGLAFAQMFTPEVGKVIMALMVMSCCGSLLGWQFTIAQV   299
               :*  .:  *: *.   :   *  :**. :   :     ..::    . .* ** .::  .*.

AdiC|P60061|   AKAAADDGLFPPIFARVNKAGTPVAGLIIVGILMTIF-----QLSSISPNATKEFGLVSS   355
CadB|P0AAE8|   GVRAANDGNFPKVYGEVDSNGIPKKGLLLAAVKMTALMILITLMNSAGGKASDLFGELTG   356
PotE|P0AAF1|   FKSSSDEGYFPKIFSRVTKVDAPVQGMLTIVIIQSGL-----ALMTISPSLNSQFNVLVN   354
               ::::*  ** ::..*  .   *  *::    : :      :. ::.: *: .:. 

AdiC|P60061|   VSVIFTLVPYLYTCAALLLLGHGHFGKAR--PAYLAVTTIAFLYCIWAVVGSGAKEVMWS   413
CadB|P0AAE8|   IAVLLTMLPYFYSCVDLIRFEGVNIRNF----VSLICSVLGCVFCFIALMGASSFELAGT   412
PotE|P0AAF1|   LAVVTNIIPYILSMAALVIIQKVANVPPSKAKVANFVAFVGAMYSFYALYSSGEEAMLYG   414
               ::*:  .::**: :  *: :     : :.  ::.:  *: .:.    :

AdiC|P60061|   FVTLMVITAMYALNYNRLHKNPYPLDAPISKD--  445
CadB|P0AAE8|   FIVSLIILMFYARKMHERQSHS--MDNHTASNAH  444
PotE|P0AAF1|   SIVTFLGWTLYGLVSPRF-----ELKNKHG----  439
               :. ::   :*.   .      :.   . 
```

Fig. S9. AdiC, CadB, and PotE are virtual proton pump exchangers from *E. coli* and members from APC superfamily. Amino acid residues discussed in the text are indicated in bold and on yellow background. Amino acid sequence alignment was performed with Clustal Omega (www.clustal.org/omega/). The UniProt ID codes of AdiC, CadB, and PotE are P60061, P0AAE8, and P0AAF1, respectively. The three characters (asterisk, colon, dot) indicate positions that have a single, fully conserved residue (*), and conservation between groups of strongly (:), and weakly similar properties (·). The strong and weak groups are defined as strong score >0.5 and weak score ≤0.5 occurring in the Gonnet PAM 250 matrix. Color coding of amino acid residues is according to their physicochemical properties: that is, small and hydrophobic (including aromatic except tyrosine) (red), acidic (blue), basic (magenta), and others (green) amino acid residues.

Fig. S10. Potential conformational changes of AdiC involved in Agm release into the periplasmic space. To illustrate the differences between outward-facing occluded (magenta; [Arg]AdiC-N22A structure, PDB ID code: 3L1L) (10) and outward-open conformations (blue; [Agm]AdiC-wt structure) of AdiC, both structures were superpositioned and are represented as cartoon ribbon (helices shown as solid cylinders). Most pronounced movements in this conformational change (indicated by yellow arrows) are within transmembrane regions, i.e., transmembrane α-helices (TMs) 2, 6 and 10. Minor differences found on the periplasmic side (top) are the result of crystal contacts; for example, the region marked by an asterisk.

Table S1.   Data collection and refinement statistics for AdiC

Data collection and refinement	[Agm]AdiC-wt	[apo]AdiC-wt
Data collection		
Wavelength (Å)	1.0	1.0
Space group	P 2_1 2_1 2	P 2_1 2_1 2
Unit-cell parameters,		
a, b, c (Å); $\alpha = \beta = \gamma$ (°)	104.8, 175.6, 72.9; 90	104.8, 175.4, 73.2; 90
Resolution (Å)	49.44–2.59 (2.73–2.59)	49.51–2.21 (2.33–2.21)
No. of observed reflections	280,724 (38,770)	401,210 (52,895)
No. of unique reflections	41,837 (5,764)	68,197 (9,571)
R_{merge} (%)	10.9 (117)	7.1 (114)
Completeness (%)	98.7 (94.9)	99.4 (96.8)
Multiplicity	6.7 (6.7)	5.9 (5.5)
$I/\sigma I$	12.0 (1.6)	14.9 (1.5)
$CC_{1/2}$ (%)	99.9 (71.3)	99.9 (58.9)
Refinement		
Resolution (Å)	49.45–2.59	49.52–2.21
R_{work}/R_{free} (%)	22.09/25.07	19.72/21.01
No. of atoms		
Protein	6,484	6,480
Ligand	18	—
Water	12	159
Mean B factor (Å^2)	68.8	60.1
Protein	68.7	60.2
Ligand	70.5	—
Water	57.3	55.8
Rmsd		
Bond length (Å)	0.007	0.007
Bond angle (°)	0.922	0.996
Ramachandran plot (%)		
Favored region	99.1	99.7
Allowed region	100	100
Disallowed region	0	0

Values in parentheses reflect the highest-resolution shell.

Movie S1.   Visualization of potential conformational changes in AdiC involved in the release of Agm into the periplasmic space of *E. coli* (see also Fig. 1*B*). The backbone of AdiC is shown as light-blue cartoon. Selected side chains of residues involved in Agm binding, occlusion and release are displayed as sticks and color labeled: N101 (orange), M104 (green), W202 (pink), I205 (brown), E208 (blue), W293 (cyan) and S357 (violet). The substrate Agm and the identified crystallographic water molecules in the substrate-binding pocket are shown as black stick model and red balls. Water molecules appearing during the morph and binding to the substrate-binding pocket originate from the bulk solution.

Movie S1